Engineering Journal issn: 0125-8281

Article

Mixing-Performance Evaluation of a Multiple Dilution Microfluidic Chip for a Human Serum Dilution Process

Therdthai Thienthong[1], Ekachai Juntasaro[1,*], Witsaroot Sripumkhai[2], Nongluck Houngkamhang[3], Mayuree Chanasakulniyom[4], Numfon Khemthongcharoen[5], Pattaraluck Pattamang[2], Nithi Atthi[2], Chamras Promptmas[5], Panapat Uawithya[6], and Wutthinan Jeamsaksiri[2]

1 Mechanical Engineering Simulation and Design Group, The Sirindhorn International Thai-German Graduate School of Engineering (TGGS), King Mongkut's University of Technology North Bangkok, Bangkok 10800, Thailand
2 Thai Microelectronics Center, National Electronics and Computer Technology Center, National Science and Technology Development Agency, Chachoengsao 24000, Thailand
3 College of Materials Innovation and Technology, King Mongkut's Institute of Technology Ladkrabang, Bangkok 10520, Thailand
4 Department of Clinical Chemistry, Faculty of Medical Technology, Mahidol University, Nakhon Pathom 73170, Thailand
5 Department of Biomedical Engineering, Faculty of Engineering, Mahidol University, Nakhon Pathom 73170, Thailand
6 Department of Physiology, Faculty of Medicine, Siriraj Hospital, Mahidol University, Bangkok 10700, Thailand
*E-mail: ekachai.j@tggs.kmutnb.ac.th (Corresponding author)

Abstract. This paper is aimed to propose a numerically designed multiple dilution microfluidic chip that can simultaneously deliver several serum dilutions in parallel. The passive mixing scheme is selected for dilution and achieved by the serpentine mixing channel in which Dean vortices are induced to increase the contact area and time for better diffusion. The mixing performance at the exit of this dilution chip is numerically evaluated using five commonly-used mixing indices with the goal that the homogeneity of the mixture over the exit cross-sectional area of the mixing channel must be greater than 93.319% to fulfill the six-sigma quality control.

Keywords: Microfluidics, dilution, mixing flow, mixing index, human serum.

1. Introduction

Human serum dilution is part of the medical diagnostics. The human blood is composed of red blood cells, white blood cells, plasma, and platelets. The serum is the plasma without fibrinogen [1]. Both serum and plasma are the Newtonian fluids [2] which are generally soluble in water. The serum consists of proteins, electrolytes, antibodies, antigens, hormones, and exogenous substances where the albumin (also called the serum albumin) is the major protein. In a dilution process, the serum is usually diluted by the phosphate buffered saline (PBS) which is a water-based salt solution consisting of sodium chloride, phosphate buffer, and potassium chloride. The PBS buffer is commonly used to dilute biological substances because it is nontoxic and isotonic. In practice, the serum is diluted in a microwell plate (typically, the 96-well plate) at multiple concentrations. This conventional technique is time consuming and requires a skilled operator and a precise tool in order to obtain accurate dilution samples when the serum is diluted at very low volume concentration. These issues can be overcome by using a microfluidic chip to improve the accuracy of the volume concentration and also to reduce the processing time. Microfluidic devices increasingly play an important role in modern medical diagnostic testing processes. One of the key functions of the microfluidic chip is a mixing function [3] which is the process of mixing a fluid sample with a buffer in a micromixer. This process is also known as a dilution process. In general, microfluidic mixing schemes can be categorized into two types: active and passive. There were two classical reviews on micromixers reported in 2005 [4, 5]. Recent advances in micromixers were reviewed in 2015 for mixing enhancement methods [6] and in 2016 exclusively for passive micromixers [7]. The active mixing scheme is the process that has the external energy/force involved to promote mixing, for instance, acoustics [8, 9], electrokinetics [10, 11, 12, 13, 14, 15, 16], thermal actuator [17], and magnetohydrodynamics [18]. The passive mixing scheme employs the geometry-specific channel to induce the chaotic advection (due to the lack of turbulence at very low Reynolds number) [19] in order to increase the contact area and contact time between the fluids to enhance mixing. Various designs of geometry-specific channels for passive mixing were proposed: the intersecting channels [20, 21, 22, 23], the convergent-divergent channels [24, 25, 26], the 3D-structure channels [27, 28, 29, 30, 31], the channels with embedded barriers [32, 33, 34, 35, 36, 37, 38], the channels with staggered herringbone structures [39], the twisted channels [40], and the Tesla-structure channels [41, 42]. Depending on applications and operations, either active or passive mixing scheme can be applied to micromixers of microfluidic systems in order to obtain the homogeneous mixture. The passive mixing scheme is chosen in this work to make the microfluidic chip user-friendly without accessories. When the microfluidic chip is operated, a small amount of fluid is manipulated inside the system and the Reynolds number

(Re) of the fluid flow in the microfluidic chip is very small (in the present work, $Re < 30$). The Reynolds number is defined as the ratio of the inertial force to the viscous force. This ratio can be written as

$$Re = \frac{Inertial\ force}{Viscous\ force} = \frac{VD_h}{\nu} = \frac{\rho VD_h}{\mu} \qquad (1)$$

where ρ is the density of fluid [kg/m³], V is the cross-section-averaged flow velocity [m/s], D_h is the hydraulic diameter of the channel [m], μ is the dynamic viscosity of fluid [Pa-s] and ν is the kinematic viscosity of fluid ($\nu = \mu / \rho$) [m²/s]. At very low Reynolds number (compared to $Re_C = 2300$, a critical Reynolds number that indicates an upper limit of the laminar flow regime), the flow behavior is dominated by the viscous force and hence the flow is highly ordered and smooth. Thus, the fluid flow in the microfluidic chip is entirely laminar or in other words the turbulent flow does not exist. This laminar flow regime results in the difficulty of mixing the fluid sample with the buffer in the microfluidic chip. The mixing performance of microfluidics depends on the diffusion between two fluids. In the published literature, there were four mixing indices (MI) commonly used to measure the mixing performance: MI_1 [43, 44], MI_2 [45, 44], MI_3 [46, 47, 44], and MI_4 [48]. MI_5 is another interesting mixing index that was also used [49], which was originally proposed as the area-weighted uniformity index [50]. These mixing indices are defined as follows:

MI_1:

$$MI_1 = \sigma = \sqrt{\frac{1}{N}\sum_{i=1}^{N}(\phi_i - \bar{\phi})^2} \qquad (2)$$

$$\bar{\phi} = \frac{\sum_{i=1}^{N}\phi_i}{N} \qquad (3)$$

where ϕ_i is the local volume concentration at the ith cell, $\bar{\phi}$ is the averaged of volume concentration over the cross-sectional area which is formulated as Eq. (3), and N is the number of cells over the same cross-sectional area. The MI_1 is also known as the standard deviation (σ) in statistics. The MI_1 reflects the level of mixing. When the MI_1 is equal to zero, it means the completely mixed state. However, when the MI_1 is higher than zero, it is at the not-well-mixed state. This MI_1 cannot be compared with other mixing indices because this mixing index does not range from 0 to 1.

MI_2:

$$MI_2 = 1 - \frac{\sigma}{\bar{\phi}} = 1 - \frac{\sqrt{\frac{1}{N}\sum_{i=1}^{N}(\phi_i - \bar{\phi})^2}}{\bar{\phi}} \qquad (4)$$

This MI_2 is the absolute mixing index which is dimensionless and ranges from 0 (unmixed) to 1 (completely mixed).

MI_3:

$$MI_3 = 1 - \frac{\sigma}{\sigma_0} = 1 - \frac{\sqrt{\frac{1}{N}\sum_{i=1}^{N}(\phi_i - \bar{\phi})^2}}{\sqrt{\frac{1}{N}\sum_{i=1}^{N}(\phi_{0,i} - \bar{\phi})^2}} \qquad (5)$$

where σ_0 is the standard deviation at the unmixed state and $\phi_{0,i}$ is the local volume concentration at the ith cell at the unmixed state. This MI_3 can be called the relative standard deviation between completely mixed and unmixed states which is scaled from 0 (unmixed) to 1 (completely mixed).

MI_4:

$$MI_4 = 1 - \frac{\iint |\phi - \bar{\phi}|\, dA}{\iint |\phi_0 - \bar{\phi}|\, dA} = 1 - \frac{\sum_{i=1}^{N}\left[\, |\phi_i - \bar{\phi}|\, A_i \right]}{\sum_{i=1}^{N}\left[\, |\phi_{0,i} - \bar{\phi}|\, A_{0,i} \right]} \qquad (6)$$

where A_i is the cross-sectional area of the ith cell and $A_{0,i}$ is the cross-sectional area of the ith cell at the unmixed state. This MI_4 is scaled from 0 (unmixed) to 1 (completely mixed).

MI_5:

$$MI_5 = 1 - \frac{\sum_{i=1}^{N}\left[\, |\phi_i - \bar{\phi}_a|\, A_i \right]}{2|\bar{\phi}_a|\sum_{i=1}^{N} A_i} \qquad (7)$$

where $\bar{\phi}_a$ is the area-weighted average of volume concentration at the cross-sectional area which is defined as

$$\bar{\phi}_a = \frac{\sum_{i=1}^{N}\phi_i A_i}{\sum_{i=1}^{N} A_i} \qquad (8)$$

This MI_5 is also known as the area-weighted uniformity index [50] which has the same scaling range as MI_2, MI_3 and MI_4 (0:unmixed to 1:completely mixed). As far as the literature survey and review is concerned with the best knowledge of the authors, MI_5 has never been used in the evaluation of mixing performance of micromixers. Therefore, this paper is aimed to propose MI_5 as a proper mixing index to evaluate the mixing performance of micromixers.

The mixing index indicates how well the mixture is homogeneous. Since there are five different definitions being used to define the mixing index, the multiple dilution microfluidic chip designed in this work will be numerically tested against these four mixing indices (MI_2, MI_3, MI_4 and MI_5) in order to evaluate its mixing performance at the exit of the chip. The challenge of designing the passive micromixer is to find an effective mechanism to increase the contact area and contact time between the fluids in the microchannel. In passive micromixers, the fluid transport can be achieved by two mechanisms: (1) the advective mechanism where the bulk movement of two fluid streams is driven by the externally applied force such as pressure-driven flow, and (2) the diffusive mechanism which is driven by entropy [51] so that the fluid molecules move randomly with this mechanism. Diffusion is considered as the statistical mechanism due to the fact that molecules move from a region of higher concentration to a region of lower concentration stochastically. From the literature survey, it is found that there are two different approaches to study the diffusion: (i) mixing of the same fluid with different concentrations and (ii) mixing of the different fluids with different viscosities, densities and concentrations. For the first approach, many researchers studied mixing of the same fluid with different concentrations in the straight microchannel, for example, for numerical and experimental study [52] and for analytical study [53]. Basically, the diffusion mechanism was investigated by mixing two fluid streams of different concentrations in the mixing channel. However, both fluid streams had the same density and viscosity because the same base fluid was employed, except that one fluid stream contained a very small amount of an extra chemical whereas the other fluid stream contained either no extra chemical or a different extra chemical in order to make their solution concentrations different. For the second approach, very few researchers investigated the diffusion phenomena between two different fluids with different viscosities, densities and concentrations, for instance, to quantitatively estimate an inter-diffusion coefficient [54] and to numerically study the mixing performance of micromixers [55]. In the current research work, the study will focus on two different fluids (serum and buffer) with different viscosities, densities and concentrations.

To enhance the contact area and contact time between the fluids for better diffusion, the curved channel can be used to induce a pair of counter-rotating secondary flows

which are known as the Dean vortices. This can help improve the diffusive mixing [56]. The Dean vortices are generated by the centripetal force at the bend. The rates of heat and mass transfer are increased when the Dean vortices are encountered. In Fig. 1, the Dean vortices appear in the curved channel. The first mathematical study of the Dean vortices was presented by W. R. Dean in 1927 and 1928 [57, 58, 59]. Dean also proposed the dimensionless number to indicate the intensity and shape of the Dean vortices. This number is known as Dean Number (Dn) which can be defined as

$$Dn = \frac{Re}{\sqrt{R/a}} \tag{9}$$

where R is the mean radius of curvature [m] and a is the width of the curved channel [m], which is illustrated in Fig. 1. Bara and co-workers conducted the experiment to visualize the Dean vortices in the curved square channel [60, 61]. They also measured the axial velocity profile in the curved square channel by using Laser Doppler Velocimetry (LDV). One pair, or even two pairs, of two counter-rotating vortices were revealed as shown in Fig. 2. In 2013, Norouzi and Biglari presented the analytical solution of the incompressible flow in the curved channel with the rectangular cross section [62]. This analytical solution can mathematically describe the Dean vortices. Recently, the Dean vortices were used to mix the serum with the buffer in the multiple dilution microfluidic chip [49].
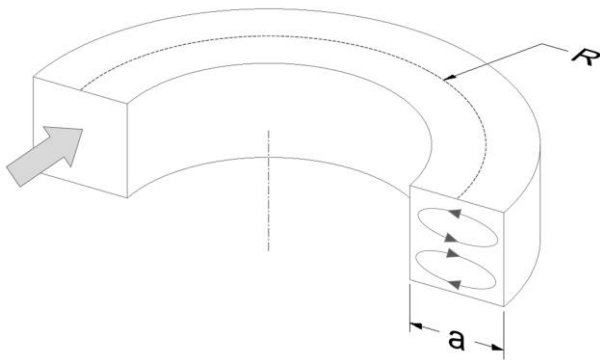

Fig. 1. Dean vortices in a curved channel.

In order to maintain the generation of the Dean vortices, the curved length of the flow passage must be continuous. There are many types of curved channels such as spiral and serpentine channels. In this paper, the serpentine channel will be considered. The serpentine curve is a series of semi-circles made alternating. An example of the serpentine channel with 10 semi-circles is shown in Fig. 3. The advantages of the serpentine channel are that the Dean number is constant and its layout can be designed to be compact in terms of the area-effective concern which is suitable for micro-scale devices. Its design is aimed to simultaneously deliver multiple serum dilutions in parallel from 1:2 to 1:32 which are the volume

concentration ratios of the serum to the PBS buffer. The CFD simulation will be used here as a measuring tool to numerically quantify the mixing indices of four different definitions (MI_2 - MI_4) in order to verify the mixing performance at the exit of the current design of the multiple dilution microfluidic chip where the homogeneity of the mixture between the serum and the PBS buffer must not be less than 93.319% (Sigma Level 3) across the cross section at the channel exit, according to the six sigma quality control [63, 64].
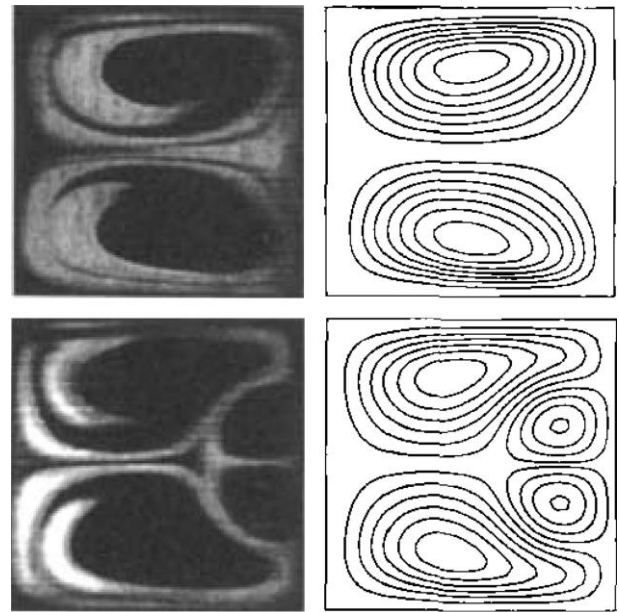

Fig. 2. Flow visualization (left) and numerical streamlines (right) of Dean vortices over a curved channel cross-section where the outer wall is on the right-hand side (referred to Bara, 1992 [61]).

2. Governing Equations

In this paper, the process of mixing the serum with the PBS buffer produces a binary liquid mixture which can be considered as the multi-component fluid flow. In order to simulate and study this fluid flow, three governing equations are required: continuity, species transport and Navier-Stokes equations. The governing equations are simplified based on the following assumptions: (1) serum, PBS and mixture are the Newtonian fluids, (2) the fluid flow is steady, incompressible and laminar, (3) there is no chemical reaction between serum and PBS, (4) the diffusivity between serum and PBS is identical due to the binary mixture process [65]. Thus, three governing equations can be written as follows:

2.1. Continuity Equation

$$\frac{\partial(\rho u)}{\partial x} + \frac{\partial(\rho v)}{\partial y} + \frac{\partial(\rho w)}{\partial z} = 0 \tag{10}$$
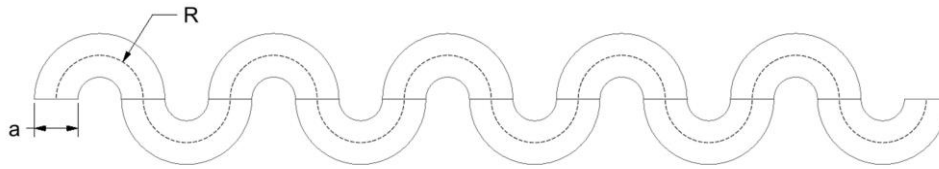
Fig. 3. Example of the serpentine channel.

where u, v, and w are the velocity components in the x-, y- and z-directions of the Cartesian coordinate system respectively and ρ is the density of mixture.

2.2. Species Transport Equation for Serum and PBS

$$\frac{\partial(\rho u \omega_s)}{\partial x} + \frac{\partial(\rho v \omega_s)}{\partial y} + \frac{\partial(\rho w \omega_s)}{\partial z} = -(\frac{\partial j_{s,x}}{\partial x} + \frac{\partial j_{s,y}}{\partial y} + \frac{\partial j_{s,z}}{\partial z}) \tag{11}$$

$$\frac{\partial(\rho u \omega_p)}{\partial x} + \frac{\partial(\rho v \omega_p)}{\partial y} + \frac{\partial(\rho w \omega_p)}{\partial z} = -(\frac{\partial j_{p,x}}{\partial x} + \frac{\partial j_{p,y}}{\partial y} + \frac{\partial j_{p,z}}{\partial z}) \tag{12}$$

where ω_s and ω_p are the mass fractions of serum and PBS respectively, j_s is the mass diffusion flux of serum and j_p is the mass diffusion flux of PBS which can be described based on the Cartesian coordinate system in the following equations.

Mass diffusion flux of serum (j_s):

$$j_{s,x} = -\mathcal{D}_{sp}\frac{\partial(\rho \omega_s)}{\partial x}$$
$$j_{s,y} = -\mathcal{D}_{sp}\frac{\partial(\rho \omega_s)}{\partial y} \tag{13}$$
$$j_{s,z} = -\mathcal{D}_{sp}\frac{\partial(\rho \omega_s)}{\partial z}$$

Mass diffusion flux of PBS (j_p):

$$j_{p,x} = -\mathcal{D}_{ps}\frac{\partial(\rho \omega_p)}{\partial x}$$
$$j_{p,y} = -\mathcal{D}_{ps}\frac{\partial(\rho \omega_p)}{\partial y} \tag{14}$$
$$j_{p,z} = -\mathcal{D}_{ps}\frac{\partial(\rho \omega_p)}{\partial z}$$

Where $\mathcal{D}_{sp}$ and $\mathcal{D}_{ps}$ are the diffusion coefficients of serum and PBS [cm²/s] respectively which are identical [65] ($\mathcal{D}_{sp} = \mathcal{D}_{ps}$). This $\mathcal{D}_{sp}$ of binary liquids can be calculated by using the following formula [66]:

$$\mathcal{D}_{sp} = 7.4 \times 10^{-8} \frac{\sqrt{\psi_p M_p T}}{\mu \tilde{V}_s^{0.6}} \tag{15}$$

where ψ_p is the association parameter for PBS ($\psi_p = 2.6$) [66], M_p is the molecular weight of PBS [g/mol], T is the absolute temperature [K], $\tilde{V}_s$ is the molar volume of the serum [cm³/mol] and μ is the viscosity of mixture [mPa-s].

2.3. Navier-Stokes equations:

$$\frac{\partial(\rho uu)}{\partial x} + \frac{\partial(\rho vu)}{\partial y} + \frac{\partial(\rho wu)}{\partial z} = -\frac{\partial p}{\partial x} + [\frac{\partial}{\partial x}\tau_{xx} + \frac{\partial}{\partial y}\tau_{yx} + \frac{\partial}{\partial z}\tau_{zx}] \tag{16}$$

$$\frac{\partial(\rho uv)}{\partial x} + \frac{\partial(\rho vv)}{\partial y} + \frac{\partial(\rho wv)}{\partial z} = -\frac{\partial p}{\partial y} + [\frac{\partial}{\partial x}\tau_{xy} + \frac{\partial}{\partial y}\tau_{yy} + \frac{\partial}{\partial z}\tau_{zy}] \tag{17}$$

$$\frac{\partial(\rho uw)}{\partial x} + \frac{\partial(\rho vw)}{\partial y} + \frac{\partial(\rho ww)}{\partial z} = -\frac{\partial p}{\partial z} + [\frac{\partial}{\partial x}\tau_{xz} + \frac{\partial}{\partial y}\tau_{yz} + \frac{\partial}{\partial z}\tau_{zz}] \tag{18}$$

where p is the pressure and τ_{ij} is the viscous stress terms which can be defined as follows:

$$\tau_{xx} = 2\mu[\frac{\partial u}{\partial x}] - \frac{2}{3}\mu[\frac{\partial u}{\partial x} + \frac{\partial v}{\partial y} + \frac{\partial w}{\partial z}] \tag{19}$$

$$\tau_{yy} = 2\mu[\frac{\partial v}{\partial y}] - \frac{2}{3}\mu[\frac{\partial u}{\partial x} + \frac{\partial v}{\partial y} + \frac{\partial w}{\partial z}] \tag{20}$$

$$\tau_{zz} = 2\mu[\frac{\partial w}{\partial z}] - \frac{2}{3}\mu[\frac{\partial u}{\partial x} + \frac{\partial v}{\partial y} + \frac{\partial w}{\partial z}] \tag{21}$$

$$\tau_{xy} = \tau_{yx} = \mu[\frac{\partial v}{\partial x} + \frac{\partial u}{\partial y}] \tag{22}$$

$$\tau_{yz} = \tau_{zy} = \mu[\frac{\partial w}{\partial y} + \frac{\partial v}{\partial z}] \tag{23}$$

$$\tau_{zx} = \tau_{xz} = \mu[\frac{\partial u}{\partial z} + \frac{\partial w}{\partial x}] \qquad (24)$$

2.4. Density and Viscosity of Mixture

In addition to the governing equations, the total mass of the binary liquid mixture is equal to unity ($\omega_s + \omega_p = 1$). Based on the binary liquid mixture, the density and viscosity can be calculated by using the following equations [50]:

Density of the binary liquid mixture (ρ):

$$\rho = \frac{1}{\frac{\omega_s}{\rho_s} + \frac{\omega_p}{\rho_p}} = \frac{\rho_s \rho_p}{\omega_s \rho_p + \omega_p \rho_s} \qquad (25)$$

where ρ_s and ρ_p are the densities of serum and PBS respectively.

Viscosity of the binary liquid mixture (μ):

$$\mu = \omega_s \mu_s + \omega_p \mu_p \qquad (26)$$

where μ_s and μ_p are the viscosities of serum and PBS respectively.

3. Simulation Setup and Validation

The finite-volume-based simulation of the flow and mixing behavior in the dilution microfluidic chip has been performed by using the commercial CFD software called ANSYS FLUENT 18.2 [50]. In this work, the validation of the simulation setup is also conducted. The first validation case is a single fluid flow in the square-cross-section straight duct and the second validation case is a single fluid flow in the square-cross-section curved duct. Geometry and dimension, mesh information, numerical methods, schemes and algorithms, convergence criteria, mechanical properties of the working fluid, Reynolds number, Dean number and flow conditions will be given in this section.

3.1. Square-cross-section Straight Duct

To begin with, the first case is to simulate the single fluid flow in the square-cross-section straight duct with one inlet and one outlet. The duct has the width and height of 100 [μm] and the duct length is 1000 [μm] long. The mesh-independent solution is the main purpose of this case study. In this case, the structured meshes of 8×8, 16×16, 32×32 and 64×64 elements are generated along the width and height of the duct. The meshes have the aspect ratio of 1, the skewness of 0 and the orthogonal quality of 1, which are in principle perfect. This mesh setup results in the total number of elements for each case: 8×8 (5,120 elements), 16×16 (40,960 elements), 32×32

(327,680 elements) and 64×64 (2,625,536 elements). The SIMPLEC (Semi-Implicit Method for Pressure Linked Equations-Consistent) algorithm is used for pressure-velocity coupling scheme. The spatial discretizations of gradient, pressure and momentum are least squares cell based, second order and second order upwind, respectively. All four mesh cases are simulated until residuals are lower than 1.0e-12 and level off. The mechanical properties of water as a working fluid are 1000 [kg/m3] for the density and 0.001 [Pas] for the dynamic viscosity. The typical volume flow rate of microfluidics is used, i.e. Q = 1 [μL/min] corresponding to Reynolds number (Re) of 0.16667. This can be converted to the constant mass flow rate of 16.667e9 [kg/s] for the inlet boundary condition. The outlet is set as the constant pressure boundary condition at 0 [Pa]. Then, the computed axial velocity profiles across the vertical symmetry plane at the outlet are compared with the exact solution [67] as shown in Fig. 4. The root-mean-square error in percentage of the axial velocity of each case is also calculated: 8×8 (6.14%), 16×16 (1.73%) 32×32 (0.46%) and 64×64 (0.15%). It can be concluded that the 32×32 and 64×64 mesh configurations with the current numerical methods, schemes and algorithms can provide the results in excellent agreement with the exact solution with the difference lower than 0.5%.
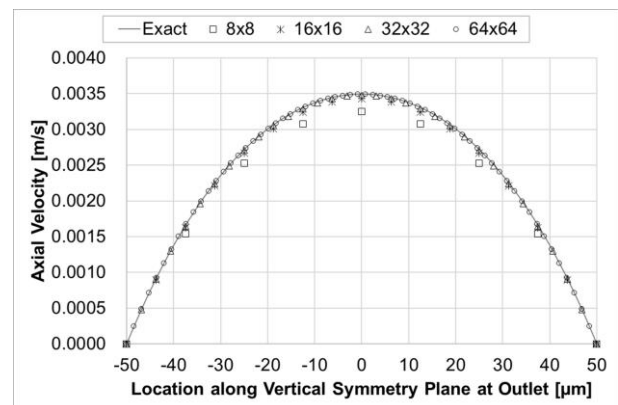

Fig. 4. Axial velocity profiles across the vertical symmetry plane of the duct outlet.

3.2. Square-cross-section Curved Duct

The single fluid flow in the square-cross-section curved duct with one inlet and one outlet is used as the second validation case. This second case is selected to validate the simulation setup in order to capture the effect of Dean vortices on the fluid flow behavior. The flow domain geometry of the simulation is created following Bara's study [60, 61], as shown in Fig. 5. The 1000-mm entrance straight duct is attached to the inlet of the curved duct whose square cross section is 12.7mm wide and high with a 270° axial arc length. The mean radius (R) of the curved duct is equal to 191.77 [mm] which is calculated from the curvature ratio (R_c) of 15.1 ($R_c = R/a$) defined in Eq. (9)). The same flow condition as Bara's study [60, 61] is defined by using Dn equal to 125 (corresponding
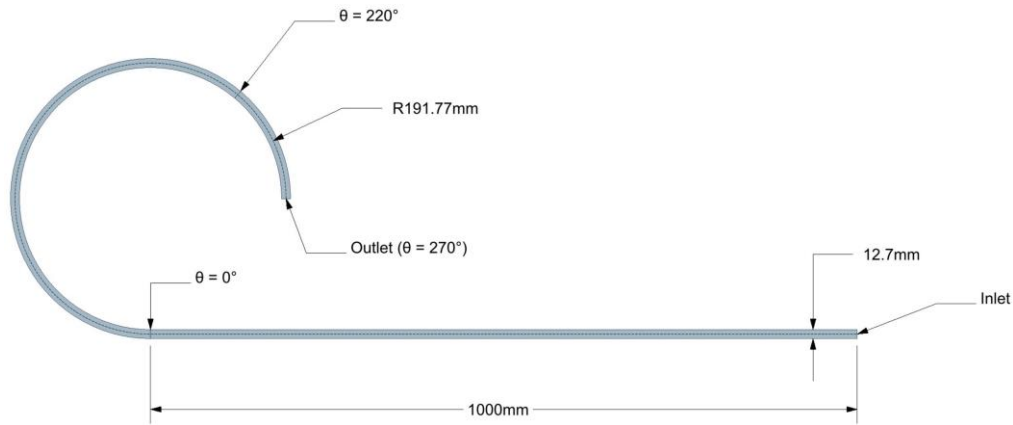
Fig. 5. Curved duct geometry.

to Re = 485.734). The structured meshes of 16×16, 32×32 and 64×64 elements are generated along the width and height of the duct cross section, which result in the averaged aspect ratio of 1, the averaged skewness of 0 and the averaged orthogonal quality of 1. The number of elements per case is 614400, 4716544, 36765696 elements, respectively. The numerical methods, schemes and algorithms, as well as the working fluid mechanical properties, are the same as those used in the first validation case. The constant mass flow rate of 0.006148361 [kg/s] is applied at the inlet which is calculated from the duct width of 12.7-mm, R_c of 15.1 and Dn of 125. The outlet is set as the constant pressure boundary condition at 0 [Pa]. The solutions of three meshes are converged with the residuals lower than 1.0e-10. The computed axial velocity profiles across the width and height of the curved duct at θ = 220° are compared with the experimental results [60, 61] and also the analytical solution [62], as shown in Fig. 6. The 32×32 and 64×64 mesh configurations provide almost the same results. It is again found that the simulation results are in good agreement with the experimental data and the analytical solution.

3.3. Dilution Microfluidic Chip

In order to increase the diffusion area between serum and PBS, the dilution chip has been designed to have three inlets with one outlet. The serpentine geometry is selected to design the mixing channel of the dilution chip. There are two major parameters to create a serpentine curved channel: the width a of the rectangular cross-section and the mean radius R, as shown in Fig. 3. The serpentine mixing channel is designed based on the curvature ratio (R_c) equal to 1 in order to gain the curve continuation and compactness with an optimized Dean number. The serpentine mixing channel of this study is an alternating connected semicircle curved channel with many folds. This results in the dilution chip with the 70-mm width and 25-mm height as shown in Fig. 7. The delivery channel inlets are indicated as Inlet 1: PBS, Inlet 2: serum and Inlet 3: PBS. The serum is fed into the middle delivery channel inlet while the PBS buffer is fed into the left and right side delivery channel inlets in order to maximize the contact

area between serum and PBS for better diffusion. The intersection angle between the PBS inlet (1) and the serum inlet (2) is 45 degrees and so is the intersection angle between the PBS inlet (3) and the serum inlet (2).
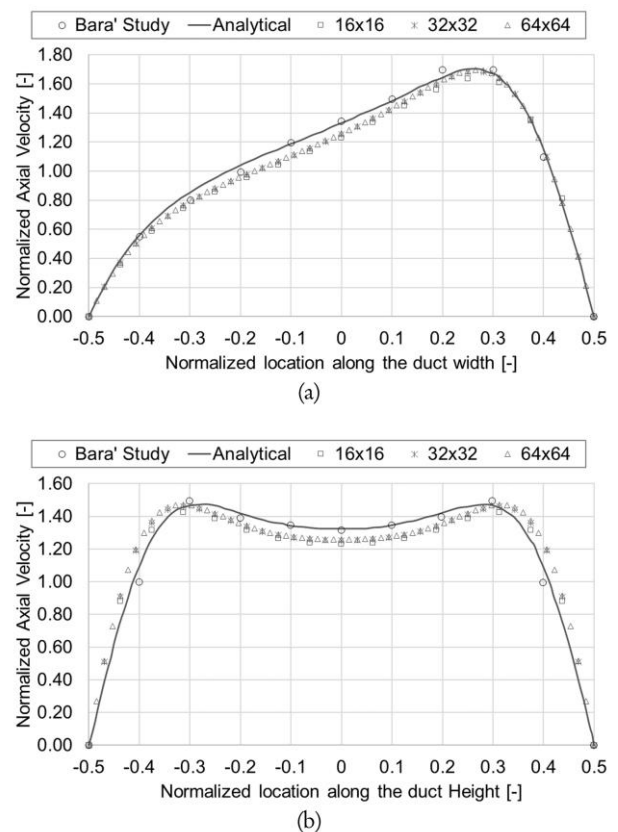

(a)

(b)

Fig. 6. Axial velocity profiles (a) along the width and (b) along the height of the curved duct at θ = 220°.
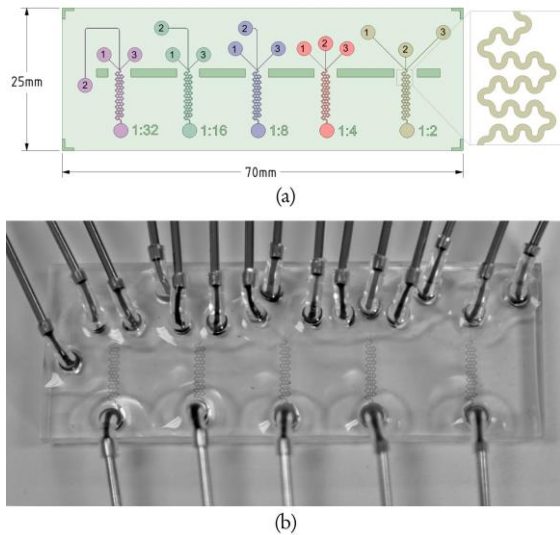
Fig. 7. Layout of 5 individual dilution channels on a chip: (a) chip drawing and (b) chip prototype.

3.3.1. Geometry and dimension

With the limitations of casting Silicon-master fabrication, all channels on the same chip essentially have the same depth of 40 μm. The three inlets of each channel have the same square cross-section width of 40 μm. The lengths of serum and PBS inlets are determined by using (having) the same pressure drop (Δp [Pa]) which is formulated as follows [67]:

$$\Delta p = 12\mu Q \frac{L}{ba^3} \frac{1}{\left[1 - \frac{192a}{\pi^5 b}\sum_{i=1,3,5,...}^{\infty}\frac{\tanh(i\pi b/2a)}{i^5}\right]} \quad (27)$$

where μ is the dynamic viscosity of fluid [Pa-s], Q is the volume flow rate [m³/s], L is the length of the channel [m], a is the width of the rectangular channel cross-section [m] and b is the height of the rectangular channel cross section [m]. When the rectangular cross-section of the channel is the same, the ratio of the pressure drop of PBS to serum inlets can be calculated by using the following equation:

$$\frac{\Delta p_p}{\Delta p_s} = \frac{\mu_p Q_p L_p}{\mu_s Q_s L_s} \quad (28)$$

where Δp_p and Δp_s are the pressure drop over PBS and serum inlets, μs and μp are the viscosities of serum and PBS, Q_s and Q_p are the volume flow rates of serum and PBS, and L_s and L_p are the lengths of serum and PBS inlets. When the pressure drops are the same, i.e. $\Delta p_p / \Delta p_s = 1$, this yields

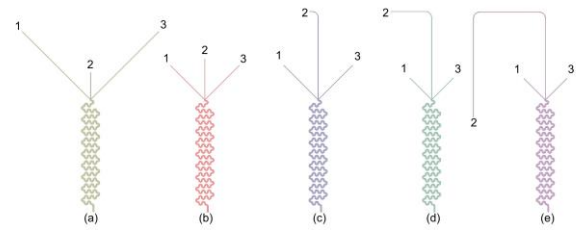$$\frac{L_s}{L_p} = \frac{\mu_p Q_p}{\mu_s Q_s} \quad (29)$$

Fig. 8. Fluid domain of volume concentration ratios: (a) 1:2, (b) 1:4, (c) 1:8, (d) 1:16 and (e) 1:32.

The lengths of all delivery channel inlets are calculated based on Eq. (29) which are summarized in Table 1. The different lengths of all delivery channel inlets are obviously shown in Fig. 8. The lengths of serum and PBS inlets are determined by using the same pressure drop in order to ensure that the mass flow rates of both serum and PBS can be delivered to the inlet of the serpentine mixing channel according to the designed amount, and hence the volume concentration ratios needed. The cross-section of the serpentine mixing channel is 120 μm wide with R_c equal to 1 and its length is 40084 μm.

Table 1. Lengths of five individual delivery channel inlets on a chip.

Volume Concentration Ratio	PBS [μm]	Serum [μm]
1:2	8000	2235
1:4	4000	3353
1:8	4000	7825
1:16	2500	10481
1:32	2500	21661

3.3.2. Mesh information

Simulations of the three-dimensional dilution channels are set up in ANSYS FLUENT release 18.2 for solving the steady laminar incompressible flow of Newtonian fluids. The fluid domains of all volume concentration ratios with three inlets and one outlet are shown in Fig. 8. Since the fluid domain in symmetrical with respect to the symmetry plane which is located in between two counter-rotating vortices, referred to Fig. 1, only the upper part of the fluid domain is considered for simulation. The fluid domain is meshed with hexahedral and prism elements by using the sweep mesh method in ANSYS meshing tool. There are typically 16 elements along the depth of the channel and 32 elements along the width of each inlet. The number of elements is maintained consistently which results in having 96 elements along the width of the serpentine mixing channel throughout downstream to the outlet. Overall, the mesh quality can be considered as a good mesh as shown in Table 2 because it is the structured mesh, except at the connecting zone between the inlets and the serpentine mixing channel where there are some unstructured mesh patterns.

Table 2.   Mesh information of the fluid domain.

		Volume Concentration Ratio				
		1:2	1:4	1:8	1:16	1:32
	Number of elements	46,226,000	43,406,928	45,237,856	45,097,056	49,677,904
Aspect Ratio "Aspect Ratio = 1" is perfect.	Min	1				
	Max	4.5684				
	Average	1.3333				
Skewness "Skewness = 0" is perfect.	Min	0				
	Max	0.51843				
	Average	0.0036				
Orthogonal Quality "Orthogonal Quality = 1" is perfect.	Min	0.5662				
	Max	1				
	Average	0.9999				

3.3.3. Numerical methods, schemes and algorithms

In terms of the numerical methods, schemes and algorithms for the simulation of mixing in the dilution chip, the SIMPLEC algorithm is used for the pressure-velocity coupling scheme. The spatial discretizations of gradient, pressure and momentum are calculated by using the least squares cell based, second order and second order upwind schemes respectively. The species transport model is setup based on the constant mass diffusion coefficient in this simulation. The solutions of all volume concentrations ratios are converged with the residuals lower than 1.0e-5.

3.3.4. Mechanical properties of serum and PBS

The mechanical properties (density and viscosity) of each fluid are required to perform mixing flow simulations. In this paper, the density and viscosity of fluids were measured by using the Density Meter DMA 4500M, Anton Paar GmbH and the Automated Micro Viscometer (AMVn), Anton Paar GmbH, respectively. The density and viscosity of serum, PBS and mixtures are given in Table 3.

Table 3. Measured mechanical properties of serum, PBS buffer and mixture at various volume concentration ratios.

Working Fluids	Density [g/cm³]	Viscosity [mPa · s]
Pure PBS	1.003674	0.925580
Pure Serum	1.024680	1.655780
1:2	1.014158	1.214060
1:4	1.008724	1.073700
1:8	1.006240	1.031100
1:16	1.004886	1.000100
1:32	1.003978	0.972600

3.3.5. Flow conditions

The exact volumes of serum and PBS buffer are required in order to correctly feed them into the delivery channel inlets and let them mix in the serpentine mixing channel with the intention of obtaining the precise volume concentration ratios. By maintaining the volume flow rate of mixture (Q_{mix}), the volume flow rates of serum and PBS can be calculated and controlled. Q_{mix} is prescribed as a constant for all volume concentration ratios in this study. Then, the volume flow rate of mixture can be expressed as

$$Q_{mix} = Q_s + Q_p \qquad (30)$$

where Q_s is the volume flow rate of serum [m³/s] and Q_p is the volume flow rate of PBS buffer [m³/s]. The

relation between the volume concentration of serum (ϕ_s) and that of PBS buffer (ϕ_p) is given as

$$\phi_s + \phi_p = 1 \tag{31}$$

Then, multiplying Eq. (31) by Q_{mix} gives

$$\phi_s Q_{mix} + \phi_p Q_{mix} = Q_{mix} \tag{32}$$

Matching Eq. (32) with Eq. (30) yields

$$\begin{aligned} Q_s &= \phi_s Q_{mix} \\ Q_p &= \phi_p Q_{mix} \end{aligned} \tag{33}$$

For example, given ϕ_s = 1/32 and the constant Q_{mix} = 128 [μL/min]. Hence, Q_s = (1/32) × 128 = 4 [μL/min] and Q_p = (31/32) × 128 = 124 [μL/min]. In this study, the serum and PBS volume flow rates of various volume concentration ratios are calculated based on Eq. (33) as summarized in Table 4. The Reynolds numbers of pure serum and pure PBS (inlets) are calculated using the measured data from Table 3 based on Eq. (1). The Reynolds numbers of the mixtures (outlets) are also calculated based on the measured data of serum and PBS in Table 3 by using the following formulation:

$$Re_{mix} = \frac{1}{2} \frac{\mu_s Re_s + \mu_p Re_p}{\mu_{mix}} \tag{34}$$

where Res, Rep and Remix are the Reynolds numbers of pure serum, pure PBS and mixture, μmix is the dynamic viscosity of the mixture. Additionally, all volume concentration ratios are designed at the same mixture volume flow rate of 128 [μL/min]. Therefore, the constant mass flow rates at three inlets and the constant pressure at outlet (Pressure = 0 [Pa]) are specified as the boundary conditions. The diffusion coefficients are independently obtained for each volume concentration ratio based on Eq. (15) as shown in Table 4. These diffusion coefficients remain constant along the flow path. In this study, the association parameter for PBS (ψ_p) is specified as 2.6 [66], the molecular weight of PBS (M_p) is 411.029 [g/mol] obtained from the National Center for Biotechnology Information [68]. According to the temperature of the testing and measuring conditions, T is equal to298.15[K]. The molar volume of the serum $\tilde{V}_s$ is equal to 64836.827 [cm³/mol] which is calculated from the molecular weight of serum (M_s = 66437 [g/mol], referred to the molecular weight of the majority protein in the serum [69]) divided by its density (as shown in Table 3). The viscosities of mixtures (μ_{mix}) are shown in Table 3. The simulation results of this dilution microfluidic chip at five volume concentration ratios will be validated against the

Table 4. Reynolds numbers of the dilution chip at inlets and outlet, volume flow rates of serum and PBS buffer and diffusion coefficients between serum and PBS buffer at various volume concentration ratios.

Volume Concentration Ratios	Re at Inlet [-]		Q at Inlets [m³/s]		Re at Outlet [-]	$\mathcal{D}_{sp}$ [cm²/s]
	PBS	Serum	PBS	Serum		
1:2	14.46	16.50	5.33333E-10	1.06667E-09	22.28	7.70471E-07
1:4	21.69	8.25	8.00000E-10	5.33333E-10	25.06	8.71191E-07
1:8	25.30	4.13	9.33333E-10	2.66667E-10	26.03	9.07184E-07
1:16	27.11	2.06	1.00000E-09	1.33333E-10	26.80	9.35304E-07
1:32	28.01	1.03	1.03333E-09	6.66667E-11	27.54	9.61750E-07

Table 5. Experimental volume concentration ratios from UV-vis absorption method and target volume concentration ratios.

Volume Concentration ratios	Serum Protein Content			
	Target Ratio	Experimental Averaged Ratio	Standard Deviation	% Diff.
1:2	0.5	0.5077	0.05297	1.54%
1:4	0.25	0.24103	0.02203	-3.59%
1:8	0.125	0.11693	0.00887	-6.45%
1:16	0.0625	0.0618	0.01182	-1.12%
1:32	0.03125	0.0332	0.00495	6.24%

experimental data and flow visualization in the next section.

4. Experimental Setup and Validation

The experiment is conducted to validate the microfluidic chip design and the operating conditions. The PDMS microfluidic chip is manufactured by casting process. For validation, the first method is the UV-vis absorption which is used to validate the volume concentration of the proposed volume flow rates and the second method is the confocal laser scanning microscopy (CLSM) which is used to visualize the flow pattern in the microfluidic chip in order to validate the flow pattern obtained from the simulation.

4.1. Fabrication of Microfluidic Chips

There are two main processes in fabricating a dilution microfluidic chip: the fabrication of the Silicon-master (Si-master) and the casting of the PDMS microfluidic chip. Beginning with the Si-master fabrication, a 6-inch Silicon-wafer (Si-wafer) is cleaned by dipping in a piranha solution in order to remove organic contaminants from the surfaces of Si-wafer. Then, the Si-wafer is spin-coated with the Hexamethyldisilazane (HMDS) and baked at 90° for 90 seconds to improve the photoresist (PR) adhesion to the oxidized Si-wafer surface. A commercially available positive PR, PFI34a (Sumitomo Corporation), is spin-coated at a rate of 1000 rpm for 20 seconds in order to obtain a thickness of approximately 2 μm on the Si-wafer, and the channel patterns are prepared by a conventional photolithography method using a mask aligner (EVG 620, EV Group). The spin-coated wafer is then exposed with 365 nm UV-light through a lithograph mask. The UV-light intensity is 40 mW/cm² and the exposed time is 5 seconds. A mask with feature sizes ranging from 40 μm to 120 μm is used. The Si-wafer is post-exposure baked at 110° for 100 seconds in order to enhance the hardening of the surface, then developed in SD-W, Sumitomo Corporation, for 75 seconds, and hard baked at 120° for 80 seconds. Afterwards, the photo-patterned Si-wafer is etched via deep reactive ion etcher (DRIE) using SF6/C4F8 gases. The remaining PR is stripped with oxygen plasma. Finally, the Si-master with 40-μm etch depth is obtained. The process schematic of manufacturing the Si-master is displayed in Fig. 9.

Consequently, a Polydimethylsiloxane (PDMS) precursor (Sylgard 184 Silicone Elastomer, Dow Corning) and a curing agent are mixed at a ratio of 10 to 1 by weight. The PDMS mixture is poured onto the Si-master and cured at 75° for 90 min. Then, the cured PDMS is released from the Si-master, cut and punched to connect silicone tubes. The PDMS cavity side is directly bonded to a glass substrate after the surface treatment. The surface treatment is done with oxygen plasma under 40 sccm of O₂ with 30 Watts for 90 seconds. The process schematic of molding and attachment is illustrated in Fig. 10.
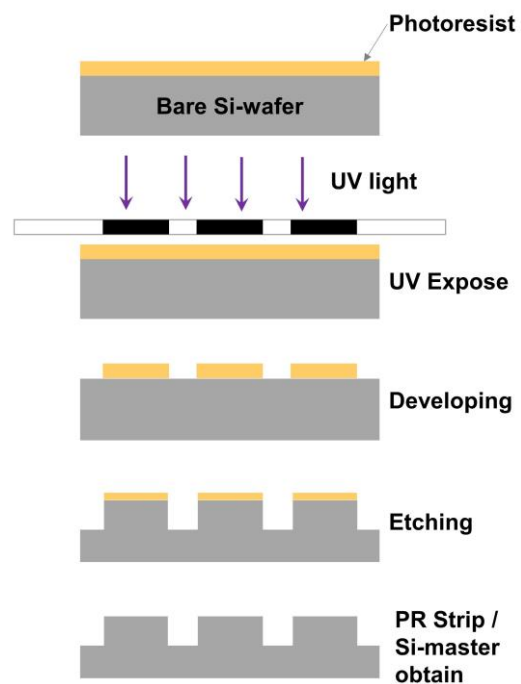

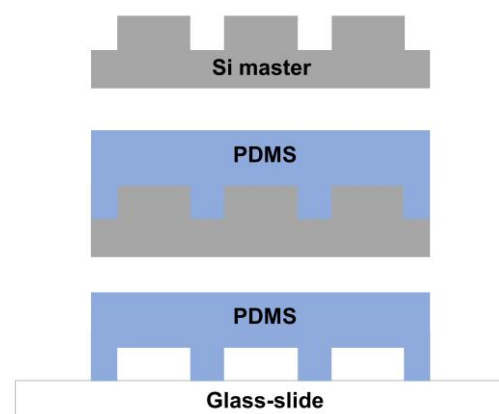Fig. 9. The Silicon-master fabrication process.

Fig. 10. The molding and attachment process of a microfluidic chip.

4.2. UV-vis Absorption Setup

The protein content in the diluted serum samples can be measured by using the UV-vis Spectrophotometer (Agilent Cary 60 UV-vis) to confirm the volume concentration ratios of the proposed volume flow rates. Pooled serum used in this study is a pooled remnant specimen collected from healthy blood donors at Siriraj hospital. The sample collection protocol was approved by Siriraj Institutional Review Board (approval number SI 330/2016). The standard curve of serum protein can be constructed by preparing various dilutions of serum protein in PBS buffer in the range of 1:100 to 1:1000 dilutions with the UV absorbance intensity at the wavelength of 280 nm of 1 mL, each of which is measured and referred to as amino acids with aromatic rings that absorb ultraviolet light. The relation between the absorbance and the concentration is plotted as a linear equation. The UV absorbance of one mL of the diluted

serum sample from the dilution chip is measured and the amount of protein absorption is calculated using the linear equation obtained. For this purpose, the protein content in the diluted serum sample is determined. The volume flow rates that are set up according to the Reynolds number in Table 4 and the feeding location in Fig. 7 are used for validation. The measured volume concentration ratios from the UV-vis absorption method are shown in Table 5 based on the three repetitions of the measurement. Based on the tested data, the variation between the target and measured volume concentration ratios is in the acceptable tolerance.

4.3. Confocal Laser Scanning Microscopy (CLSM) Setup

An Olympus UPLSAPO 10X2 objective (10x magnification), together with an Olympus FV 1000 sw confocal laser scanning microscope (CLSM), is used to visualize the mixing flow pattern in the dilution microfluidic chip. The fluorescein isothiocyanate (FITC; excitation/emission maxima = 490/525 nm) with the concentration of 0.0025 mM is added into serum in order to facilitate the visualization of fluid flow pattern in the dilution microfluidic chip. The fluorescent serum and PBS buffer (pH7.4) are introduced into the dilution microfluidic chip (as shown in Fig. 7) via the serum inlet (2) and the PBS buffer inlets (1 and 3), respectively. The fluorescent serum diffuses continuously into the PBS buffer along the serpentine dilution channel. The data acquisition and signal processing are controlled by the supplied Olympus software. Micrographs of fluid flow pattern are analyzed using ImageJ version 1.51w (March 2018). In this study, there is only one scanning zone per serpentine dilution channel immediately after the inlet junction to scan the fluid flow pattern as shown in Fig. 11.
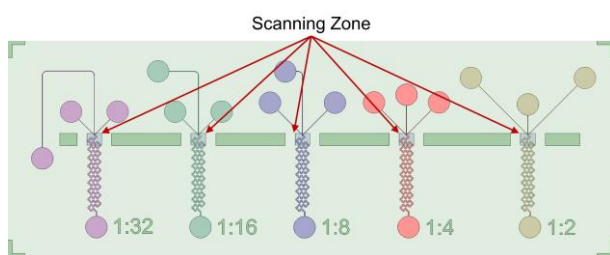

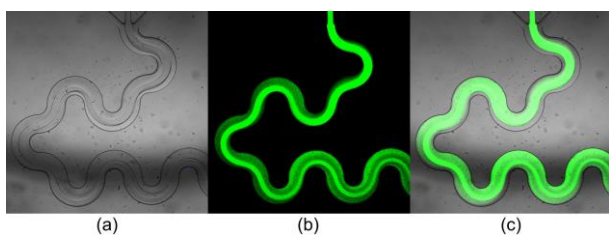Fig. 11. Scanning zones of CLSM for five volume concentration ratios.

Fig. 12. Example of CLSM scanning results: (a) BF image, (b) FITC image and (c) merged image.
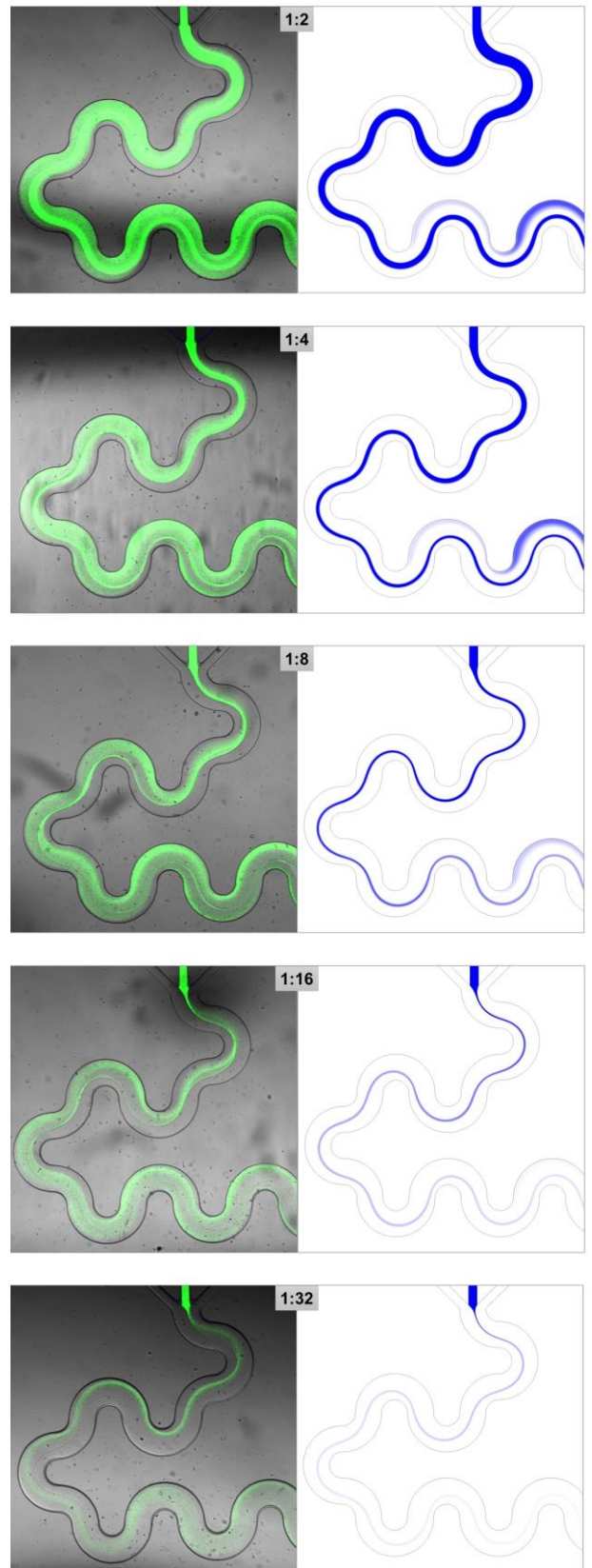

Fig. 13. Serum flow patterns: (left) CLSM results and (right) simulation results.

There are three scanning results obtained from the CLSM: the bright field (BF) result, the FITC scanning result and the merged result between the BF and FITC images. An example of BF, FITC and merged images is shown in Fig. 12. The merged images of CLSM scanning

results are compared with the simulation results in Fig. 13 in which the simulated serum flow patterns are visualized by blue color. Based on the comparison, both simulated and scanned serum flow patterns are in good agreement for all volume concentration ratios. Therefore, based on the validation results with the UV-vis absorption and CLSM methods, the proposed volume flow rates and simulation setup can be used to mimic the mixing flow inside the dilution microfluidic chip.
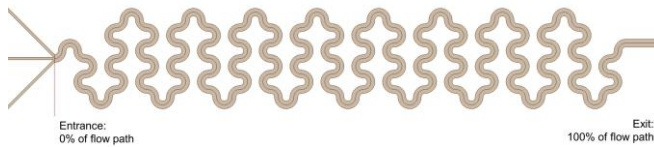
5. Evaluation of Mixing Performance

Fig. 14. Flow path length of the serpentine mixing channel.

The MI_2, MI_3, MI_4, MI_5 are calculated along the serpentine mixing channel from the entrance (0% of flow path) to the exit (100% of flow path) as shown in Fig. 14. Before the discussion below, the volume concentration ratio of 1:2 is identified as the highest one that is considered here whereas the lowest volume concentration ratio in this work is 1:32.
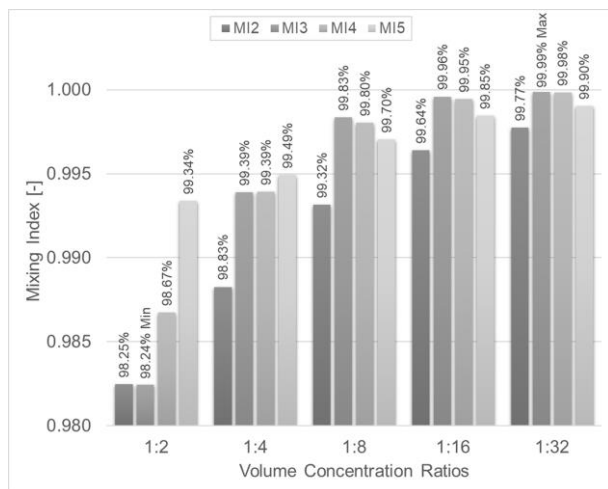

Fig. 15. Mixing index of various volume concentration ratios at the outlet.

Fig. 15 reveals the mixing index values of various volume concentration ratios at the outlet of the serpentine mixing channel where the four different definitions of the mixing index found in the literature (MI_2, MI_3, MI_4, MI_5) are adopted in the present work to numerically evaluate the mixing performance of each volume concentration ratio. It is found that the current design of the serpentine mixing channel can achieve the Sigma Level 3 where all the mixing indices obtained are well above 93.319%. The minimum value of the mixing index is gained by the MI_3 definition at the volume concentration

ratio of 1:2 while the maximum value can be reached up to 99.99% by the MI_3 definition at the volume concentration ratio of 1:32. The most demanding case for the mixing effort is the 1:2 volume concentration ratio case which is sensibly realistic because the amount of the serum is volumetrically equal to that of the PBS buffer and hence great effort is needed compared to the more diluted volume concentration ratios. With all mixing index definitions, at the volume concentration ratio of 1:2, the mixing indices obtained are rather scattered over a wide range from 98.24% to 99.34% (i.e. a deviation of 0.44) whereas the mixing index results become concentrated around 99.77%-99.99% (i.e. a deviation of 0.09) at the volume concentration ratio of 1:32. As the volume concentration ratio is more diluted from 1:2 to 1:32, the mixing index is increased for all the mixing index definitions.

Table 6. Summary of the percentage of the total flow path length to reach the mixing index of 93.319%.

93.319%	MI2	MI3	MI4	MI5
1:2	67.674	67.639	64.382	54.377
1:4	65.471	54.647	54.277	51.960
1:8	63.654	44.848	45.912	49.977
1:16	60.197	29.005	34.774	46.753
1:32	58.900	19.775	21.958	46.237

Table 6 shows a summary of the percentage (%) of the total flow path length that each mixing index can reach 93.319% to accomplish the requirement of the Sigma Level 3 at various volume concentration ratios. At the volume concentration ratio of 1:2, the mixing process needs the longest distance to achieve the Sigma Level 3 compared to other volume concentration ratios for all mixing indices. The longest distance of all required to achieve the Sigma Level 3 is indicated by MI_2, i.e. 67.67417% of the total flow path length.

On the other hand, the shortest distance is found at the volume concentration ratio of 1:32 where the shortest distance of all needed to satisfy the Sigma Level 3 is detected by MI_3, i.e. 19.77491%. The mixing index definition MI_2 is the most demanding measure of the mixing process because the required distance for the Sigma Level 3 is longest compared to the other mixing index definitions. The detected distances by MI_3 and MI_4 rather spread wide in a similar fashion over a wide range of the mixing operation, for instance, from 19.77491% (at 1:32) to 67.63863% (at 1:2) in case of MI_3, which are not attractive as mixing indices to design the micro-mixing device. However, MI_2 and MI_5 seem to be the appropriate mixing indices because the detected distances are focused in a narrow band (a distance band of 8.77447 for MI_2; 8.14052 for MI_5). From the practical point of
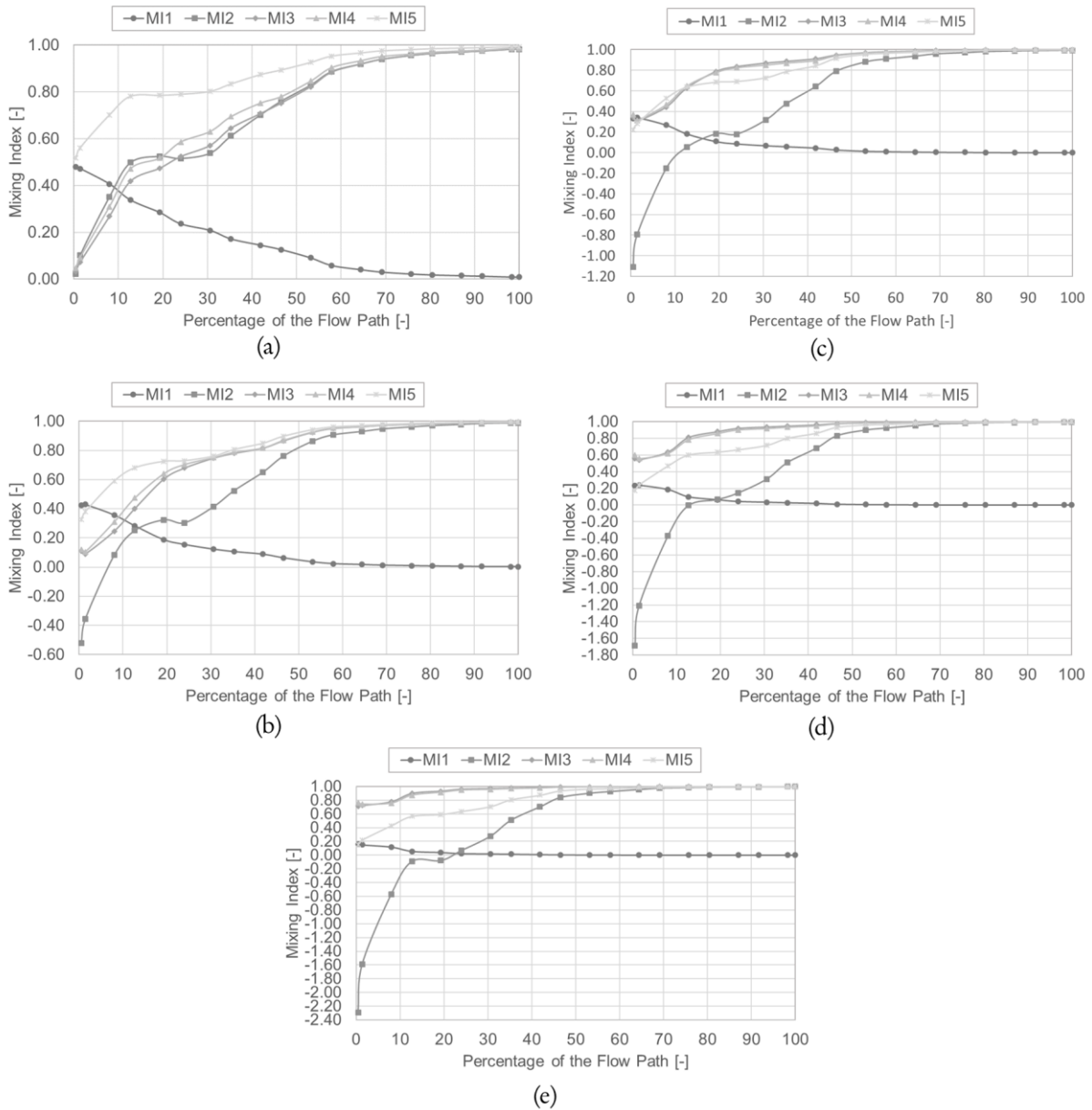
Fig. 16. Mixing index distribution along the serpentine mixing channel at various volume concentration ratios: (a) 1:2, (b) 1:4, (c) 1:8, (d) 1:16 and (e) 1:32.

view, if the regulation for processing a homogeneous mixture is strict, MI_2 becomes obviously a better choice. Fig. 16(a) – 16(e) demonstrate the distributions of the five mixing indices (MI_1, MI_2, MI_3, MI_4 and MI_5) along the serpentine mixing channel at the five different concentration ratios of 1:2, 1:4, 1:8, 1:16 and 1:32 respectively. In general, the variation trends of the MI_2, MI_3, MI_4 and MI_5 are quite similar, that is, their values at the inlet keep increasing with the distance along the mixing channel towards unity at the outlet. The distributions of MI_2 and MI_5 along the mixing channel are somewhat stationary, or in other words, do not alter much over a wide range of volume concentration ratios, where the distributions of MI_2 and MI_5 can be seen as a lower bound and an upper bound respectively. The distributions of MI_3 and MI_4 along the mixing channel

are almost the same where their inlet values vary drastically from almost zero at the volume concentration ratio of 1:2 to above 0.7 at the volume concentration ratio of 1:32. Unlike MI_2, MI_3, MI_4 and MI_5, the MI_1 varies from the maximum value at the inlet to zero at the outlet.

In Fig. 17, the mixing index MI_1 is plotted along the serpentine mixing channel at the five different volume concentration ratios (1:2, 1:4, 1:8, 1:16 and 1:32). It is found that the MI_1 at the inlet monotonically decreases along the mixing channel towards zero at the outlet for all the volume concentration ratios. At the inlet, the maximum value systematically decreases with decreasing volume concentration ratio. It implies that the more diluted the volume concentration ratio, the shorter the mixing distance is required.
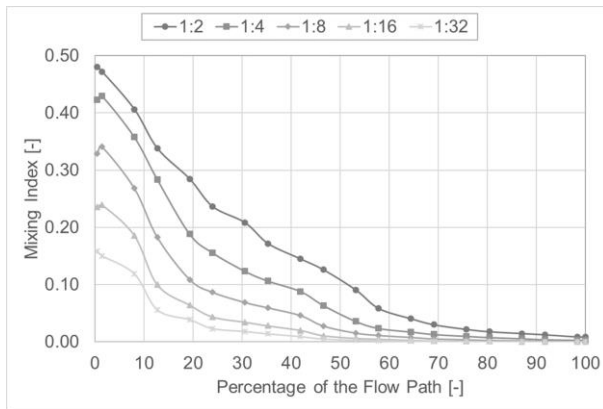
Fig. 17. Mixing index MI1 of various volume concentration ratios.

Fig. 19. Mixing index MI3 of various volume concentration ratios.

The variations of the mixing index MI_2 along the mixing serpentine channel are shown in Fig. 18 at various volume concentration ratios. It can be seen that the MI_2 at the inlet increases along the mixing channel towards unity at the outlet for all the volume concentration ratios. The inlet value is lowest at the volume concentration ratio of 1:32 and increases with increasing volume concentration ratio. However, the MI_2 provides the negative values around the entrance length as highlighted by the shaded zone. If the mixing index is meant to be defined from zero to unity, the MI_2 would be disqualified as a candidate to evaluate the mixing performance of micro-mixers.
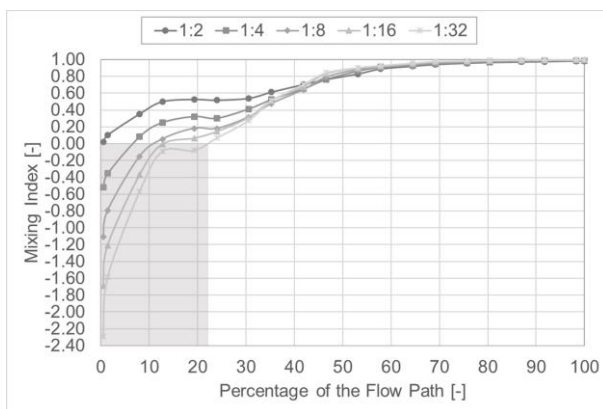
In Fig. 19 and 20, the mixing indices MI_3 and MI_4, respectively, at several volume concentration ratios vary in a similar manner where their values at the inlet increase along the mixing channel towards unity at the outlet for all the volume concentration ratios. It is interesting to note that their values near the inlet (less than 15% of the flow path) are almost identical in case of the volume concentration ratios of 1:2 and 1:4 while with the volume concentration ratios of 1:8, 1:16 and 1:32, their inlet values increase respectively. Nevertheless, it is noteworthy here that their values around the inlet experience a small dip at some volume concentration ratios, for example, 1:4, 1:8, 1:16 in case of MI_3 and 1:4, 1:8, 1:16, 1:32 in case of MI_4.
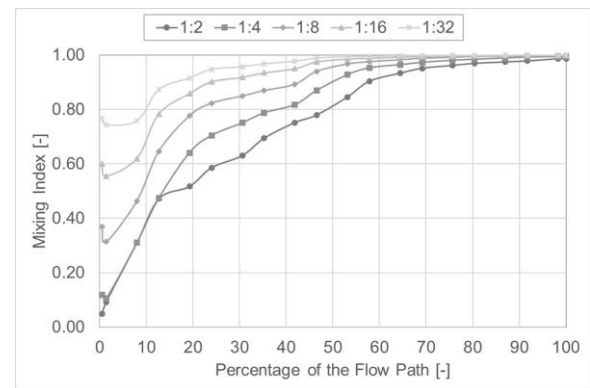

Fig. 20. Mixing index MI4 of various volume concentration ratios.

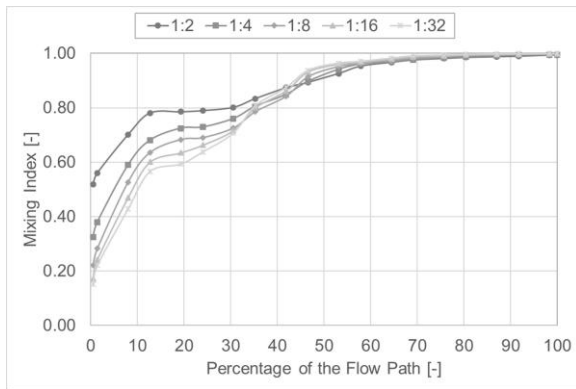Fig. 18. Mixing index MI2 of various volume concentration ratios.

Fig. 21. Mixing index MI5 of various volume concentration ratios.

In Fig. 21, the distributions of the mixing index MI_5 are shown along the serpentine mixing channel at five volume concentration ratios of interest. It is found that the MI_5 at the inlet increases along the mixing channel towards unity at the outlet for all the volume concentration ratios without any negative value or dip near the inlet. In contrast to MI_3 and MI_4, the MI_5 at the inlet increases when the volume concentration ratio is increased from 1:32 to 1:2.

Up to now, it is evident from the numerical results of all the five mixing indices shown so far that the MI_5 seems to be a good candidate to assess the mixing performance when micro-mixers are designed. The MI_5 is attractive because it is always positive with a unity value for fully mixed solution and not much sensitive to the varying concentration of the mixture over a range of the volume concentration ratio considered.

6. Conclusion

In this paper, the passive mixing/dilution microfluidic chip is proposed to mix the serum with the PBS buffer. This dilution chip with five serpentine mixing channels can deliver 1:2 up to 1:32 volume concentration ratio in parallel. Based on the CFD simulation results, at 98.24% of MI_3, the minimum mixing performance at the most effort-demanding volume concentration ratio of 1:2 can achieve the expectation of the six-sigma level 3. The MI_5 is the most attractive mixing index to assess the mixing performance of the dilution microfluidic chip due to the fact that the MI_5 is less sensitive to the volume concentration ratio and always a positive value. When the mixing performance determined by the MI_5 is considered, all five volume concentration ratios can reach above 99.0%. Thus, the proposed dilution chip can simultaneously deliver the mixture of serum and PBS buffer at five volume concentration ratios with the high level of homogeneity.

Acknowledgement

References

[1] D. A. Rubenstein, W. Yin, and M. D. Frame, *Biofluid Mechanics*, 2nd ed. Elsevier, 2015.

[2] C. K. Dixit and A. Kaushik, *Microfluidics for Biologists: Fundamentals and Applications*, C. K. Dixit and A. Kaushik, Eds. Springer International Publishing, 2016.

[3] J. M. Ottino and S. Wiggins, "Introduction: Mixing in microfluidics," *Philosophical Transactions of the Royal Society of London. Series A: Mathematical, Physical and Engineering Sciences*, vol. 362, no. 1818, pp. 923–935, May 2004. [Online]. Available: https://royalsocietypublishing.org/doi/10.1098/rsta.2003.1355.

[4] N.-T. Nguyen and Z. Wu, "Micromixers—A review," *Journal of Micromechanics and Microengineering*, vol. 15, no. 2, pp. R1–R16, Feb. 2005.

[5] V. Hessel, H. Löwe, and F. Schönfeld, "Micromixers - A review on passive and active mixing principles," *Chemical Engineering Science*, vol. 60, no. 8-9 SPEC. ISS., pp. 2479–2501, 2005.

[6] K. Ward and Z. H. Fan, "Mixing in microfluidic devices and enhancement methods," *Journal of Micromechanics and Microengineering*, vol. 25, no. 9, p. 94001, 2015.

[7] C. Y. Lee, W. T. Wang, C. C. Liu, and L. M. Fu, "Passive mixers in microfluidic systems: A review," *Chemical Engineering Journal*, vol. 288, pp. 146–160, 2016.

[8] D. Ahmed, X. Mao, B. K. Juluri, and T. J. Huang, "A fast microfluidic mixer based on acoustically driven sidewall-trapped microbubbles," *Microfluidics and Nanofluidics*, vol. 7, no. 5, pp. 727–731, 2009.

[9] T.-D. Luong, V.-N. Phan, and N.-T. Nguyen, "High-throughput micromixers based on acoustic streaming induced by surface acoustic wave,"

Microfluidics and Nanofluidics, vol. 10, no. 3, pp. 619–625, 2011.

[10] M. Campisi, D. Accoto, F. Damiani, and P. Dario, "A soft-lithographed chaotic electrokinetic micromixer for efficient chemical reactions in labon-chips," *Journal of Micro-Nano Mechatronics*, vol. 5, no. 3, pp. 69–76, 2009.

[11] C. K. Chen and C. C. Cho, "Electrokinetically driven flow mixing utilizing chaotic electric fields," *Microfluidics and Nanofluidics*, vol. 5, no. 6, pp. 785–793, 2008.

[12] C. Y. Lim, Y. C. Lam, and C. Yang, "Mixing enhancement in microfluidic channel with a constriction under periodic electro-osmotic flow," *Biomicrofluidics*, vol. 4, no. 1, p. 014101, Jan. 2010.

[13] Y. Du, Z. Zhang, C. H. Yim, M. Lin, and X. Cao, "A simplified design of the staggered herringbone micromixer for practical applications," *Biomicrofluidics*, vol. 4, no. 2, 2010.

[14] Z. Zhang, C. H. Yim, M. Lin, and X. Cao, "Quantitative characterization of micromixing simulation," *Biomicrofluidics*, vol. 2, no. 3, 2008.

[15] Y. C. Lam, H. Y. Gan, N. T. Nguyen, and H. Lie, "Micromixer based on viscoelastic flow instability at low Reynolds number," *Biomicrofluidics*, vol. 3, no. 1, 2009.

[16] M. Z. Huang, R. J. Yang, C. H. Tai, C. H. Tsai, and L. M. Fu, "Application of electrokinetic instability flow for enhanced micromixing in crossshaped microchannel," *Biomedical Microdevices*, vol. 8, no. 4, pp. 309–315, 2006.

[17] B. Xu, T. N. Wong, N. T. Nguyen, Z. Che, and J. C. K. Chai, "Thermal mixing of two miscible fluids in a T-shaped microchannel," *Biomicrofluidics*, vol. 4, no. 4, 2010.

[18] Y. Wang, J. Zhe, B. T. Chung, and P. Dutta, "A rapid magnetic particle driven micromixer," *Microfluidics and Nanofluidics*, vol. 4, no. 5, pp. 375–389, 2008.

[19] A. D. Stroock, S. K. Dertinger, A. Ajdari, I. Mezić, H. A. Stone, and G. M. Whitesides, "Chaotic mixer for microchannels," *Science*, vol. 295, no. 5555, pp. 647–651, 2002.

[20] M. A. Ansari, K.-Y. Kim, K. Anwar, and S. M. Kim, "A novel passive micromixer based on unbalanced splits and collisions of fluid streams," *Journal of Micromechanics and Microengineering*, vol. 20, no. 5, 2010.

[21] C. K. Chung, T. R. Shih, B. H. Wu, and C. K. Chang, "Design and mixing efficiency of rhombic micromixer with flat angles," *Microsystem Technologies*, vol. 16, no. 8-9, pp. 1595–1600, Aug. 2010.

[22] M. A. Ansari and K.-Y. Kim, "Mixing performance of unbalanced split and recombine micomixers with circular and rhombic sub-channels," *Chemical Engineering Journal*, vol. 162, no. 2, pp. 760–767, 2010.

[23] J. J. Chen and Y. S. Shie, "Interfacial configurations and mixing performances of fluids in staggered curved-channel micromixers," *Microsystem Technologies*, vol. 18, no. 11, pp. 1823–1833, 2012.

[24] A. Afzal and K.-Y. Kim, "Passive split and recombination micromixer with convergent-divergent walls," *Chemical Engineering Journal*, vol. 203, pp. 182–192, 2012.

[25] M. Khosravi Parsa, F. Hormozi, and D. Jafari, "Mixing enhancement in a passive micromixer with convergent-divergent sinusoidal microchannels and different ratio of amplitude to wave length," *Computers and Fluids*, vol. 105, pp. 82–90, 2014.

[26] A. Afzal and K.-Y. Kim, *Convergent-Divergent Micromixer Coupled with Pulsatile Flow*. Elsevier B.V., 2015, vol. 211.

[27] H. M. Xia, Z. P. Wang, Y. X. Koh, and K. T. May, "A microfluidic mixer with self-excited 'turbulent' fluid motion for wide viscosity ratio applications," *Lab on a Chip*, vol. 10, no. 13, p. 1712, 2010.

[28] T. W. Lim, Y. Son, Y. J. Jeong, D.-Y. Yang, H.-J. Kong, K.-S. Lee, and D.-P. Kim, "Threedimensionally crossing manifold micro-mixer for fast mixing in a short channel length," *Lab on a Chip*, vol. 11, no. 1, pp. 100–103, 2011.

[29] Y. Lin, X. Yu, Z. Wang, S. T. Tu, and Z. Wang, "Design and evaluation of an easily fabricated micromixer with three-dimensional periodic perturbation," *Chemical Engineering Journal*, vol. 171, no. 1, pp. 291–300, 2011.

[30] J. Yang, L. Qi, Y. Chen, and H. Ma, "Design and fabrication of a three dimensional spiral micromixer," *Chinese Journal of Chemistry*, vol. 31, no. 2, pp. 209–214, 2013.

[31] M. Nimafar, V. Viktorov, and M. Martinelli, "Experimental comparative mixing performance of passive micromixers with H-shaped sub-channels," *Chemical Engineering Science*, vol. 76, pp. 37–44, 2012.

[32] S. H. Wong, P. Bryant, M. Ward, and C. Wharton, "Investigation of mixing in a cross-shaped micromixer with static mixing elements for reaction kinetics studies," *Sensors and Actuators B: Chemical*, vol. 95, no. 1-3, pp. 414–424, 2003.

[33] J. M. Park, K. D. Seo, and T. H. Kwon, "A chaotic micromixer using obstruction-pairs," *Journal of Micromechanics and Microengineering*, vol. 20, no. 1, 2010.

[34] B. S. Kim, B. S. Kwak, S. Shin, S. Lee, K. M. Kim, H. I. Jung, and H. H. Cho, "Optimization of microscale vortex generators in a microchannel using advanced response surface method," *International Journal of Heat and Mass Transfer*, vol. 54, no. 1-3, pp. 118–125, 2011.

[35] L. Y. Tseng, A. S. Yang, C. Y. Lee, and C. Y. Hsieh, "CFD-based optimization of a diamond-obstacles inserted micromixer with boundary protrusions," *Engineering Applications of Computational Fluid Mechanics*, vol. 5, no. 2, pp. 210–222, 2011.

[36] Y. Fang, Y. Ye, R. Shen, P. Zhu, R. Guo, Y. Hu, and L. Wu, "Mixing enhancement by simple periodic geometric features in microchannels," *Chemical Engineering Journal*, vol. 187, pp. 306–310, 2012.

[37] S. J. Wu, H. C. Hsu, and W. J. Feng, "Novel design and fabrication of a geometrical obstacleembedded

micromixer with notched wall," *Japanese Journal of Applied Physics*, vol. 53, no. 9, 2014.

[38] H. Le The, H. Le Thanh, T. Dong, B. Q. Ta, Tran-Minh, and F. Karlsen, "An effective pas-sive micromixer with shifted trapezoidal blades using wide Reynolds number range," *Chemical Engineering Research and Design*, vol. 93, pp. 1–11, 2015.

[39] C. A. Cortes-Quiroz, A. Azarbadegan, M. Zangeneh, and A. Goto, "Analysis and multi-criteria design optimization of geometric characteristics of grooved micromixer," *Chemical Engineering Journal*, vol. 160, no. 3, pp. 852–864, 2010.

[40] Y. Zhang, Y. Hu, and H. Wu, "Design and simulation of passive micromixers based on capillary," *Microfluidics and Nanofluidics*, vol. 13, no. 5, pp. 809–818, 2012.

[41] S. Hossain, M. A. Ansari, A. Husain, and K.-Y. Kim, "Analysis and optimization of a micromixer with a modified Tesla structure," *Chemical Engineering Journal*, vol. 158, no. 2, pp. 305–314, 2010.

[42] A. S. Yang, F. C. Chuang, C. K. Chen, M. H. Lee, S. W. Chen, T. L. Su, and Y. C. Yang, "A highperformance micromixer using three-dimensional Tesla structures for bio-applications," *Chemical Engineering Journal*, vol. 263, pp. 444–451, 2015.

[43] R. Liu, M. Stremler, K. Sharp, M. Olsen, J. Santiago, R. Adrian, H. Aref, and D. Beebe, "Passive mixing in a three-dimensional serpentine microchannel," *Journal of Microelectromechanical Systems*, vol. 9, no. 2, pp. 190–197, Jun. 2000.

[44] A. Hashmi and J. Xu, "On the Quantification of Mixing in Microfluidics," *Journal of Laboratory Automation*, vol. 19, no. 5, pp. 488–491, Oct. 2014.

[45] H. C. Tekin, V. Sivagnanam, A. T. Ciftlik, A. Sayah, C. Vandevyver, and M. A. M. Gijs, "Chaotic mixing using source–sink microfluidic flows in a PDMS chip," *Microfluidics and Nanofluidics*, vol. 10, no. 4, pp. 749–759, Apr. 2011.

[46] S. Wang, X. Huang, and C. Yang, "Mixing enhancement for high viscous fluids in a microfluidic chamber," *Lab on a Chip*, vol. 11, no. 12, p. 2081, 2011.

[47] H. V. Phan, M. B. Coşkun, M. Şeşen, G. Pandraud, A. Neild, and T. Alan, "Vibrating membrane with discontinuities for rapid and efficient microfluidic mixing," *Lab on a Chip*, vol. 15, no. 21, pp. 4206–4216, 2015.

[48] M. Du, Z. Ma, X. Ye, and Z. Zhou, "On-chip fast mixing by a rotary peristaltic micropump with a single structural layer," *Science China Technological Sciences*, vol. 56, no. 4, pp. 1047–1054, 2013.

[49] T. Thienthong, E. Juntasaro, W. Sripumkhai, N. Houngkamhang, M. Chanasakulniyom, N. Khemthongcharoen, M. Yasawong, C. Hruanun, A. Poyai, C. Promptmas, P. Uawithya, and W. Jeamsaksiri, "Design and validation of a multiple dilution microfluidic chip for a human serum preparation," in *The 7th Thai Society of Mechanical Engineers – International Conference on Mechanical Engineering*, Dec. 2016.

[50] ANSYS, *ANSYS Fluent Theory Guide Release 18.2*. ANSYS, Inc., 2017.

[51] J. Castillo-Leo'n and W. E. Svendsen, *Lab On-A-Chip Devices and Micro-Total Analysis Systems*, J. Castillo-León and W. E. Svendsen, Eds. Springer International Publishing, 2015.

[52] J. M. Chen, T. L. Horng, and W. Y. Tan, "Analysis andmeasurementsofmixinginpressure-drivenmicrochannel flow," *Microfluidics and Nanofluidics*, vol. 2, no. 6, pp. 455–469, 2006.

[53] H. Song, Y. Wang, and K. Pant, "Cross-stream diffusion under pressure-driven flow in microchannels with arbitrary aspect ratios: A phase diagram study using a three-dimensional analytical model," *Microfluidics and Nanofluidics*, vol. 12, no. 1-4, pp. 265–277, 2012.

[54] J. Dambrine, B. Géraud, and J. B. Salmon, "Interdiffusion of liquids of different viscosities in a microchannel," *New Journal of Physics*, vol. 11, 2009.

[55] M. A. Ansari and K.-Y. Kim, "A numerical study of mixing in a microchannel with circular mixing chambers," *AIChE Journal*, vol. 55, no. 9, pp. 2217–2225, Sep. 2009.

[56] D. Di Carlo, "Inertial microfluidics," *Lab on a Chip*, vol. 9, no. 21, pp. 3038–3046, 2009.

[57] W. Dean, "XVI. Note on the motion of fluid in a curved pipe," *The London, Edinburgh, and Dublin Philosophical Magazine and Journal of Science*, vol. 4, no. 20, pp. 208–223, Jul. 1927.

[58] W. R. Dean, "Fluid Motion in a Curved Channel," *Proceedings of the Royal Society A: Mathematical, Physical and Engineering Sciences*, vol. 121, no. 787, pp. 402–420, 1928.

[59] W. Dean, "LXXII. The stream-line motion of fluid in a curved pipe (Second paper)," *The London, Edinburgh, and Dublin Philosophical Magazine and Journal of Science*, vol. 5, no. 30, pp. 673–695, Apr. 1928.

[60] B. Bara, "Experimental investigation of developing and fully developed flow in a curved duct of square cross section," Ph.D. dissertation, University of Alberta, 1991.

[61] B. Bara, K. Nandakumar, and J. H. Masliyah, "An experimental and numerical study of the Dean problem: flow development towards twodimensional multiple solutions*," Journal of Fluid Mechanics*, vol. 244, pp. 339–376, 1992.

[62] M. Norouzi and N. Biglari, "An analytical solution for Dean flow in curved ducts with rectangular cross section," *Physics of Fluids*, vol. 25, no. 5, p. 053602, 2013.

[63] C. Gygi, B. Williams, and S. R. Covey, *Six Sigma for Dummies*, 2nd ed. John Wiley & Sons, Inc, 2012.

[64] B. S. El-Haik, *Axiomatic Quality*. Hoboken, NJ, USA: John Wiley & Sons, Inc., Mar. 2005.

[65] R. B. Bird, E. N. Lightfoot, and W. E. Stewart, *Transport Phenomena*, 2nd ed. John Wiley & Sons, 2002.

[66] C. R. Wilke and P. Chang, "Correlation of Diffusion Coefficients in Dilute Solutions," *AIChE Journal*, vol. 1, no. 2, pp. 264–270, 1955.

[67] F. M. White, *Viscous Fluid Flow*, 3rd ed. McGraw-Hill Education, 2006.

[68] National Center for Biotechnology Information, "Phosphate-Buffered Saline Information," 2008.

[Online]. Available: https://pubchem.ncbi.nlm.nih.gov/compound/24978514

[69] Sigma-Aldrich, "Human Albumin," 1996. [Online]. Available: https://www.sigmaaldrich.com/ life-science/metabolomics/enzyme-explorer/ enzyme-reagents/human-albumin.html

---

Therdthai Thienthong received B.Eng. degree in mechanical engineering from Kasetsart University, Thailand, in 2003. He received M.Sc. in mechanical engineering simulation and design from The Sirindhorn International Thai-German Graduate School of Engineering (TGGS), King Mongkut's University of Technology North Bangkok (KMUTNB), Thailand, in 2013. He has been a Doctoral candidate in mechanical engineering of The Sirindhorn International Thai-German Graduate School of Engineering (TGGS), King Mongkut's University of Technology North Bangkok (KMUTNB), Thailand, since 2015. He receives the tuition-fee-waiving scholarship of TGGS, KMUTNB, during his doctoral study. His research interests focus on computational fluid dynamics (CFD) and microfluidics.

Ekachai Juntasaro received B.Eng. degree in mechanical engineering from King Mongkut's Institute of Technology Ladkrabang (KMITL), Thailand in 1989, and pursued both M.Sc. and Ph.D. degrees in mechanical engineering at Imperial College London, U.K. in 1992 and 1997 respectively with the Royal Thai Government Scholarship. In 1997, he started working as Lecturer at School of Mechanical Engineering, Institute of Engineering, Suranaree University of Technology (SUT), Nakhon Ratchasima, Thailand where he became Assistant Professor and Associate Professor in 2001 and 2006 respectively. Since 2008, he has worked as Associate Professor in Mechanical Engineering Simulation and Design (MESD) Group at The Sirindhorn International Thai-German Graduate School of Technology (TGGS), King Mongkut's University of Technology North Bangkok (KMUTNB), Thailand. His research interests are unstructured finite volume method for computational fluid dynamics (CFD), transition and turbulence modelling with/without analytical wall function (AWF), microfluidics and turbomachinery flow in power plants.

Witsaroot Sripumkhai received M.S. degree in science and nanotechnology from College of Nanotechnology, KMITL, Thailand. He is currently a Senior Assistant Researcher in Surface and Microfluidic Device Innovation Research Team at Thai Microelectronics Center (TMEC), NECTEC, NSTDA. His research interests are microfabrication process for microfluidic applications and superhydrophobic surface for antifouling application.

Nongluck Houngkamhang received her Bachelor's degree with 2nd Class Honor in chemistry from Naresuan University, Thailand, in 2006. In 2007, she won the Royal Golden Jubilee Ph.D. Program scholarship granted by Thailand Research Fund to pursue her graduate study at Mahidol University, Thailand, and received her Ph.D. in materials science and engineering in 2012. In 2012, she started working as Research Associate at Mahidol University, Thailand. Since 2014, she has worked as Lecturer at College of Nanotechnology, King Mongkut's Institute of Technology Ladkrabang (KMITL), Thailand, and became Assistant Professor in 2018. She was awarded as the 8th HOPE Meeting Fellow (Japan) in 2016. Her research interests are biosensors, surface plasmon resonance, protein/DNA chips, surface chemistry, and medical diagnostic devices and kits.

Mayuree Chanasakulniyom received B.Sc. degree (Honor) in Medical Technology from Chiang Mai University, Chiang Mai, Thailand, in 2005, and M.Sc. degree in Molecular Biology and Genetic Engineering from Mahidol University, Nakhon Pathom, Thailand, in 2008. She also received Ph.D. degree in Biomedical Engineering from University of Glasgow, Glasgow, Scotland, in 2014. She is currently a Lecturer at Department of Clinical Chemistry, Faculty of Medical Technology, Mahidol University, Nakhon Pathom, Thailand. Her research interests are the medical diagnosis using lab-on-a-chip and microfluidics and the development of quality control material for quality assurance in medical diagnosis.

Numfon Khemthongcharoen received her Bachelor's and Master's degrees in medical technology from Mahidol University, Bangkok, Thailand. She has worked as a Research Assistant at National Electronics and Computer Technology Center (NECTEC), Thailand, since 2010. In 2015, she won the Royal Golden Jubilee Ph.D. Program scholarship granted by the Thailand Research Fund. She is a Ph.D. candidate in Department of Biomedical Engineering, Faculty of Engineering Mahidol University. Her research interests are biosensors, bio-optics, microfluidic system, and optical devices for medical diagnosis.

Pattaraluck Pattamang received M.S. degree in science and nanotechnology from College of Nanotechnology, KMITL, Thailand. She is currently an Assistant Researcher in Surface and Microfluidic Device Innovation Research Team at Thai Microelectronics Center (TMEC), NECTEC, NSTDA. Her research interests are Microfluidic device and Lab on a disk.

Nithi Atthi received his Bachelor's degree in Materials Engineering and Master's degree in Engineering Management from Kasetsart University (KU) in 2004 and 2008. In 2013, he won the MEXT Monbukagakusho scholarship granted by Japanese Government to pursue his graduate study at Tokyo Institute of Technology and received his Master's degree and Ph.D. in Electronics and Applied Physics. He was awarded as the Green Talent Fellow (Germany) in 2018, the 10th HOPE Meeting Fellow (Japan) in 2018, and the Young Leaders of the 16th STS forum (Japan) in 2019. He has authored and co-authored of more than 30 technical journal publications, gave a talk on his research in more than 110 academic conferences, and filed 25 domestic and international patents. In 2018, he was appointed as a Research Team Leader of Surface and Microfluidic Device Innovation Research Team at Thai Microelectronics Center (TMEC), Thailand. His research focuses on Si-based semiconductor process technology, micro/nano patterning, high-k/metal gate stacks, microfluidic devices, and superamphiphobic and anti-fouling surface by surface texturing and modification for various applications.

Chamras Promptmas received B.Sc. degree (Honor) in Medical Technology from Mahidol University, Bangkok, Thailand, in 1976, and M.Sc. Degree in Biochemistry from Chulalongkorn University, Bangkok, Thailand, in 1980. He received Diploma in Biotechnology from University of Kent at Canterbury, U.K., in 1988, and Ph.D. degree in Biochemistry from Mahidol University in 1994. He had worked on biosensor at Mahidol University for over 15 years and collaborated the research with the Fraunhofer Institute for Biosensor Research, Muenster, Germany, the Fraunhofer Institute for Biomedical Engineering, Potdam-Golm, Germany, and Department of Analytical Biochemistry, Institute of Biochemistry and Biology, University of Potsdam, Germany. Recently, he has joined Department of Biomedical Engineering, Mahidol University, as Director of Biosensors and Micro Total Analysis System Laboratory. He has expanded his work to Ion Sensitive Field Effect Transistor (ISFET) and microfluidic systems.

Panapat Uawithya received Bachelor of Science degree in Medical Science (Second Class Honors) and then Ph.D. degree in Molecular Biology and Genetic Engineering from Mahidol University, Bangkok, Thailand, in 1996 and 2001 respectively. He also received MD degree (Siriraj Hospital) from Mahidol University, Bangkok, Thailand, in 2004. He had been trained as postdoctoral research fellow at National Institutes of Health, Bethesda, MD, USA from 2006 to 2009. He has joined Department of Physiology, Faculty of Medicine, Siriraj Hospital, Mahidol University, since 2005 where he became Assistant Professor and Associate Professor in 2011 and 2019 respectively. His research interests are water channel functions and regulations in human, and biomarkers for detection of demyelinating diseases.

Wutthinan Jeamsaksiri received his M.Eng. and Ph.D. from department of electrical and electronic engineering, Imperial College London, U.K., in 1996 and 2003 respectively. He then worked as a process integration engineer on a European project at IMEC, Leuven, Belgium, from 2000 to 2004. The project he carried out was on Integration of Microwave Performance Advanced CMOS Technology. From 2005, he has been working at Thai Microelectronics Center (TMEC) under the National Electronics and Computer Technology Center (NECTEC). In 2018, he took the position as a research group director of TMEC. His work interest includes Si based sensors, MEMS, microfluidic devices, and surface texturing and modification for various applications.